Int. J. Heat Mass Transfer. Vol. 34, No. 8, pp. 2133–2147, 1991
Printed in Great Britain

0017-9310/91 $3.00 + 0.00

Heat transfer to a row of impinging circular air jets including the effect of entrainment

R. J. GOLDSTEIN and W. S. SEOL
Mechanical Engineering Department, University of Minnesota, Minneapolis, MN 55455, U.S.A.

(*Received* 11 *June* 1990 *and in final form* 12 *October* 1990)

Abstract—An experimental investigation is performed to characterize the convective heat transfer from a flat surface to a row of impinging, circular, submerged air jets formed by square-edged orifices having a length/diameter ratio of unity. Distributions of recovery factor, effectiveness, and local heat transfer coefficient are determined. Spanwise-average and surface-average heat transfer coefficients are calculated from the local heat transfer coefficients. The heat transfer coefficient is independent of the temperature difference between the jet and the ambient, if it is defined with the difference between the (heated) wall temperature and the adiabatic wall temperature. The effectiveness is independent not only of the temperature difference between the jet and the ambient but also of the jet Reynolds number in the range studied. Spanwise-average and surface-average heat transfer coefficients have the largest values on the impingement line and decrease with increasing distance away from it.

INTRODUCTION

JET IMPINGEMENT has become well established as a high performance technique for heating, cooling, or drying a surface. Applications of impinging jets include the drying of paper, textiles, and film deposited on substrates, the processing of glass and some metals, the freezing of tissue in cryosurgery, and the cooling of electronic components. Impinging jets are used to cool critical gas turbine parts such as the inner wall in the leading edge region of gas turbine blades and the outer wall of combustors.

Recently, an innovative method has been proposed to improve the performance of a gas turbine by minimizing the gap between the end of the blades and the shroud, reducing the leakage during start up and shut down. The gap can be minimized by controlling the temperature of the shroud and its thermal expansion using impinging jets. A single row of jets with jet-to-jet spacing between 5 and 40 jet diameters may be used for the control system. The distance from the jet exit to the shroud wall is between 5 and 15 jet diameters, and the ratio of the jet temperature to the temperature of the gas into which the jet discharges is between 0.5 and 1.5. The present study is inspired by this application.

When a submerged jet is discharged at a temperature different from that of the surroundings, this temperature difference affects the heat transfer from a surface to an impinging jet. Depending on the separation distance between the jet nozzle-exit and the target surface, the jet may approach the surface at a temperature that can be significantly different from its nozzle-exit value. As a result, the adiabatic wall temperature on the surface may have a different distribution from that encountered, if the jet were discharged at the same temperature as that of the surroundings. The concept of effectiveness has been borrowed from film cooling to express the adiabatic wall temperature in a dimensionless form. When the jet total temperature at the nozzle-exit is equal to the ambient temperature, the adiabatic wall temperature is defined as the recovery temperature, which is quite different from the jet total temperature when the jet velocity is large.

In the present study, recovery factor, effectiveness, and heat transfer coefficient distributions for a single row of circular air jets are investigated. The jet exit geometry is square-edged, and the exit diameter of each jet is 6.35 mm. The flow from the spent air is confined by two side walls in order to have results without significant end effects. The range of parameters is

$$2 \leqslant L/D \leqslant 8$$

$$S/D = 4, 8$$

$$10\,000 \leqslant Re \leqslant 40\,000$$

$$0 \leqslant z/D \leqslant 6.$$

Average Nusselt numbers are determined from the numerical integration of the local Nusselt number. A power law dependence of the local and the average Nusselt numbers on the jet Reynolds number is observed.

PREVIOUS STUDIES

Gardon and Cobonpue [1] first used the difference between the (impingement) plate temperature and the recovery temperature as the thermal driving force for convective heat transfer, and measured the recovery temperatures of a single, round, impinging jet for various jet exit-to-plate distances ($1 \leqslant L/D \leqslant 30$).

NOMENCLATURE

B	slot width
C_p	specific heat of fluid
D	jet exit diameter (6.35 mm in the present study)
h	heat transfer coefficient, $q_w/(T_w - T_{aw})$
k	thermal conductivity
L	jet exit to impingement plate distance
M	blowing rate, $\rho_j u_j/\rho_\infty u_\infty$
Nu	local Nusselt number, hD/k
$\overline{Nu}$	spanwise-average Nusselt number, equation (8)
$\overline{\overline{Nu}}$	surface-average Nusselt number, equation (10)
Pr	Prandtl number
q_w	convective wall heat flux
Re	jet Reynolds number, $u_j D/\nu$ or $u_j B/\nu$
r	recovery factor, $(T_r - T_j^s)/T_j^d = 1 + (T_r - T_j^o)/T_j^d$
S	jet center-to-center spacing ($4D$ and $8D$ in the present study)
Sc	Schmidt number
Sh	local Sherwood number
$\overline{Sh}$	spanwise-average Sherwood number
T_{aw}	adiabatic wall temperature
$T_{aw,0}$	adiabatic wall temperature at impingement point
T_j^d	jet dynamic temperature, $u_j^2/2C_p$
T_j^s	jet static temperature
T_j^o	jet total temperature
T_r	recovery temperature ($= T_{aw}$ when $T_j^o = T_\infty$)
T_{ref}	reference temperature
T_w	wall temperature
T_∞	ambient temperature
u_j	average jet exit velocity
u_∞	free stream velocity
x	spanwise location from impingement point of one of the central jets (Fig. 1)
z	streamwise location from impingement line (Fig. 1).

Greek symbols

η	effectiveness, $(T_{aw} - T_\infty)/(T_j^o - T_\infty)$
η^*	effectiveness, $(T_{aw} - T_\infty)/(T_j^o - T_\infty)$
ν	kinematic viscosity
ρ_j	density of jet fluid
ρ_∞	density of free stream fluid.

Goldstein *et al.* [2] studied the recovery factor distribution with a single, round, impinging jet for various jet Reynolds numbers ($61\,000 \leqslant Re \leqslant 124\,000$) and jet exit-to-plate spacings ($L/D = 2, 4, 5, 6, 7, 10, 12$). They showed the recovery factor is independent of the jet Reynolds number but is dependent on jet exit-to-plate distance. They also found that significant local minima in the recovery factor occur near stagnation ($R/D \approx \pm 2$) for small jet exit-to-plate spacings ($L/D \leqslant 4$), which can be attributed to energy separation in the highly curved flow as discussed by Eckert [3]. Bouchez and Goldstein [4], Sparrow *et al.* [5], and Goldstein and Behbahani [6] measured the recovery factor with a single, circular, impinging jet in a cross flow for various jet blowing rates (mass velocity of jet/mass velocity of flow), and found that the recovery factor is insensitive to the blowing rate, when the blowing rate is large ($M \geqslant 8$). Hollworth and Berry [7] and Behbahani and Goldstein [8] investigated the distribution of recovery temperature with an array of circular, impinging jets. Florschuetz and Su [9] measured the recovery factor distribution for an array of circular jets in a cross flow, and showed that the recovery factor is essentially independent of the jet Reynolds number except, in some cases, for the most upstream row of the array.

Several experimental studies (e.g. refs. [10–13]) have been made of the heat transfer to impinging, heated air jets, but the thermal entrainment effect has not been explicitly investigated in these studies. Bouchez and Goldstein [4] measured the local impingement effectiveness and heat transfer coefficient over the interaction area of a heated air jet impinging on a flat plate and subjected to a cross flow of air, and found that the effectiveness increases with the blowing rate when the blowing rate is small ($M \leqslant 12.5$). Folayan and Whitelaw [14] measured and calculated the effectiveness and the heat transfer coefficient for a heated slot jet impinging on a flat plate. They also investigated the influence of impingement angle and a shroud plate on the effectiveness and the heat transfer coefficient. Striegl and Diller [15, 16] measured local heat transfer rates with single and multiple slot jets issuing into an environment at a temperature between the initial temperature of the jet and the heated impingement plate temperature, and developed an analytical model to correlate the measured heat transfer rates. Hollworth and Wilson [17] measured the adiabatic wall temperature for a single, circular, heated jet impinging on a flat plate and found that the radial profiles of dimensionless adiabatic wall temperature $(T_{aw} - T_\infty)/(T_{aw,0} - T_\infty)$ are similar for large jet exit-to-plate distances ($L/D \geqslant 5$), when the radial distance is normalized by dividing by the 'arrival' value of the jet half width. They also developed a theoretical model to predict the variation of adiabatic wall temperature associated with the fully developed wall-jet. In the same apparatus, Hollworth and Gero

[18] investigated local heat transfer and found that the local heat transfer coefficient does not depend explicitly upon the temperature difference between the jet and the ambient, if the heat transfer coefficient is defined in terms of the difference between the (heated) wall temperature and the local adiabatic wall temperature. Florschuetz and Su [19] investigated the effect of the initial cross flow air temperature on impingement surface heat fluxes. The definition of effectiveness is slightly different among these researchers.

Obot *et al.* [20, 21] found that the effect entrainment has on heat transfer to a turbulent jet is strongly dependent on nozzle configuration. Most of the published literature pertains to jets generated with well-rounded convergent nozzles. However, in many industrial applications, the square-edged nozzle configuration is preferred primarily because of ease of fabrication and installation, especially when working with multiple-jet systems.

Even though impinging jets have been extensively studied for several decades, only a few researchers investigated a single row of impinging jets. Metzger *et al.* [22] measured the average Stanton number for a line of circular jets impinging on a concave surface. Koopman and Sparrow [23] used a naphthalene sublimation technique to measure the local Sherwood number for a row of impinging jets. Goldstein and Timmers [24] used a visualization technique with liquid crystals to measure the heat transfer coefficient distribution for a line of three impinging jets. A study including the effect of thermal entrainment for a single row of impinging jets is not available.

According to Gaunter *et al.* [25], a jet is fully turbulent at a jet Reynolds number near 4000 based on the jet exit diameter and average jet exit velocity. A survey of literature on impingement heat transfer is available [26].

EXPERIMENTAL APPARATUS AND MEASUREMENT PROCEDURE

Apparatus

Only a brief description of the apparatus is given here; a more complete presentation is given in ref. [27].

A building compressor provides air at a pressure of 830 ± 10 kPa (8.3 ± 0.1 bar) for the jets. After filtration, the air is regulated to a pressure not exceeding 310 kPa (3.1 bar), and the pressure fluctuations introduced by the compressor are reduced. The flow is further controlled by three needle valves in parallel. The air is metered by a sharp-edged orifice, and the temperature of the air is controlled in a 127 cm long heater section downstream of the flow metering orifice. The air is then fed into a large plenum chamber which consists of 5.08 cm thick aluminum chips and a 15.24 cm thick honeycomb section. The uniformity of the plenum temperature is checked by a thermocouple probe which can traverse horizontally through the plenum chamber. From the plenum chamber, the air is distributed to the individual orifices on the jet orifice plate via vinyl tubes and stainless steel delivery tubes. The mass flow rate of each individual jet is assumed to be equal (the variation in the jet centerline velocities is within 2%). The jet total temperature is measured 5.6 cm upstream of the nozzle-exit with two 36 gauge iron–constantan thermocouples installed near the centerline of the delivery tubes, one of which is located in the center of the row and the other in an end tube.

Figure 1 shows details of the test section, the jet exit assembly and the coordinate system. The origin ($x = 0$, $z = 0$) is denoted by 'o', x denotes spanwise position and z the streamwise position.

The orifice plate is a narrow aluminum bar ($2.54 \times 2.29 \times 57.2$ cm) with a single row of 16 square-edged orifices. The jet diameter, D, is 6.35 mm, and the distance between adjacent jets is four jet diameters. The length/diameter ratio of each jet orifice is unity. This dimension was chosen to approximate the conditions in turbine blade or combustor wall cooling. In such applications, the diameter of the hole is not too different from the thickness of the orifice plate.

Two styrofoam side walls are attached to the jet orifice plate to model a row of jets of large spanwise (x) extent so that end effects would not affect the measurements. The flow from the spent air is forced to exhaust in the streamwise (z) direction by the side walls. The distance between the inner surface of a side wall and the center of its closest jet is $S/2$. Four sets of side walls with different heights are used according to the desired jet exit-to-plate spacing (L/D).

The test plate is 24.05 cm long and 40.64 cm wide. Its bottom wall is made of a 1.6 mm thick textolite plate backed by 5 cm thick styrofoam. This provides a well-insulated back surface which ensures that the majority of the generated heat flux is convected into the jet (heat flux conducted through the back surface is less than 0.5% of the generated heat flux). Four stainless steel heating foils, 0.0254 mm thick and 5.04 cm wide, are glued to the textolite plate with a silicone rubber compound. The heating foils are separated by approximately 0.2 mm and connected in series through copper bus bars. The wall temperatures are measured with 36 gauge iron–constantan thermocouples embedded in the textolite plate and in contact with the silicone rubber compound used for glueing the heating foils to the textolite plate. Copper oxide is used as a cement and as an electrical insulator between the silicone rubber compound and the thermocouple leads. Forty thermocouples are located on one line in the center of the test plate (nominally $z = 0$), and the jet orifice plate can be set at different streamwise positions to get off-impingement-line data.

A Fluke 8520A digital multimeter with a resolution of 1 μV ($\approx 0.02^{\circ}$C) and a Fluke 2205A switch controller are used to read the thermocouple outputs. A Hewlett–Packard 85 micro-computer is employed to control the switcher and the multimeter and to send data to a PDP11/34 mini-computer.

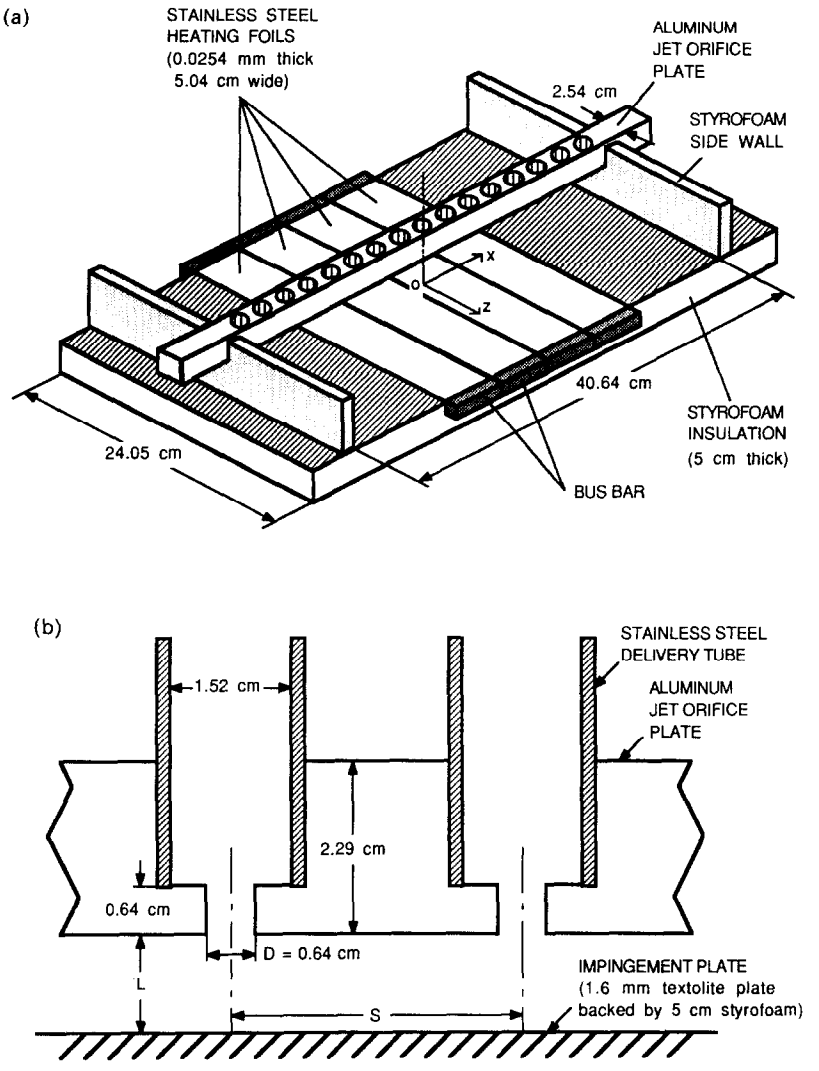

FIG. 1. Experimental apparatus: (a) test section; (b) jet exit assembly.

Experimental procedure

A complete data set for a given Re and geometric configuration requires a series of three runs: (1) recovery factor, (2) effectiveness, and (3) heat transfer coefficient. While all 16 jets are used for effectiveness and heat transfer coefficient measurements, only the inner eight jets are used for recovery factor measurements to permit a sufficiently large jet velocity so that the recovery factor could be obtained without significant experimental error. The jet Reynolds number at this flow rate is about 40 000. For the runs with large jet-to-jet spacing ($S/D = 8$), every other jet is closed off.

The recovery temperature distribution on the test plate is measured when the wall heat flux is zero and the air temperature is controlled so that

$$T_j^\circ \approx T_\infty .$$

The jet total temperature is assumed to be at the room temperature if their difference is 0.1°C or less. After the measurement is completed at the impingement line ($z/D = 0$), the jet orifice plate is moved to make measurements at subsequent streamwise locations ($z/D = 1, 2, 4, 6$). Measurements are made after steady state is reached. For the first measurement, approximately 2–3 h are required to reach steady state. However, for subsequent measurements less than 30 min are required.

The air flow is heated for the adiabatic wall temperature (effectiveness) measurements so that the jet total temperature is 5–10°C above room temperature, and the same procedure is used as in the recovery temperature measurements.

In order to measure the heat transfer coefficient distribution, the air flow and the current through the heating foils are started. After reaching steady state, a test procedure similar to that for the recovery temperature measurements is followed. In addition, the voltage drop across each heating foil and the current are measured to provide the energy dissipation in

each foil. The generated wall heat flux is corrected for radiation, conduction to the back, and lateral conduction along the test plate. The total correction is less than 5 W m^{-2} for the wall heat flux of 1700 W m^{-2}. The power level was selected so that the assumption of a constant property flow would be valid.

Error analysis

The experimental uncertainties are calculated using the method of Kline and McClintock [28]. According to the analysis [27], the uncertainty for the recovery factor is not more than 4%, that for the effectiveness is not more than 4%, and that for the Nusselt number is not more than 7%.

RESULTS AND DISCUSSIONS

Definitions

The heat transfer coefficient is generally defined by

$$h = \frac{q_w}{T_w - T_{ref}} \tag{1}$$

where q_w is the convective wall heat flux, T_w the wall temperature measured in the presence of heating, and T_{ref} a reference temperature. Several researchers have used the jet total temperature (T_j^o) as a reference temperature, while others have used the local adiabatic wall temperature (T_{aw}). Bouchez and Goldstein [4] showed that the heat transfer coefficient is independent of the wall heat flux if T_{aw} is used as T_{ref}. Hollworth and Gero [18] and Goldstein *et al.* [29] have shown that the use of T_{aw} as T_{ref} renders the heat transfer coefficient which is independent of the difference between the jet total temperature (T_j^o) and the ambient temperature (T_∞).

The local heat transfer coefficient in the present study is defined by

$$h = \frac{q_w}{T_w - T_{aw}} \tag{2}$$

and the Nusselt number is defined by

$$Nu = \frac{hD}{k} \tag{3}$$

where q_w is the wall heat flux corrected for radiation, conduction to the back, and lateral conduction along the test plate. The definition of the heat transfer coefficient based on ($T_w - T_{aw}$) is well established for flows where temperature recovery exists on the adiabatic wall [1, 2, 4, 6, 17, 18].

The adiabatic wall temperature (T_{aw}) depends on many quantities including the jet exit-to-plate distance (L/D) and the difference between the total temperature of the jet (T_j^o) and the ambient temperature (T_∞). The effectiveness, which is modified somewhat from that commonly used in film cooling studies, is defined by

$$\eta = \frac{T_{aw} - T_r}{T_j^o - T_\infty} \tag{4}$$

where T_r is the recovery temperature (for the same flow conditions and geometry) measured on the adiabatic wall when the total temperature of the jet and room air are kept equal (i.e. $T_j^o = T_\infty$). Note that ($T_{aw} - T_r$) goes to zero when ($T_j^o - T_\infty$) goes to zero.

A different definition of the effectiveness has been employed by Folayan and Whitelaw [14] and Hollworth and Wilson [17]

$$\eta^* = \frac{T_{aw} - T_\infty}{T_j^o - T_\infty}. \tag{5}$$

If the velocity of the jet is small, T_r approaches T_∞, and the two definitions converge.

The recovery temperature (T_r) is dependent on the mass flow rate of the jet (Re), the jet exit-to-plate distance (L/D), the jet-to-jet spacing (S/D), etc. The recovery temperature is expressed in a dimensionless form by defining a recovery factor (r)

$$r = \frac{T_r - T_j^s}{T_j^d} = 1 + \frac{T_r - T_j^o}{T_j^d} \tag{6}$$

where the dynamic temperature (T_j^d) of the jet is defined by

$$T_j^d = \frac{u_j^2}{2C_p}. \tag{7}$$

Periodicity

Figure 2 illustrates the spanwise periodicity and the absence of end effects in the central region of the

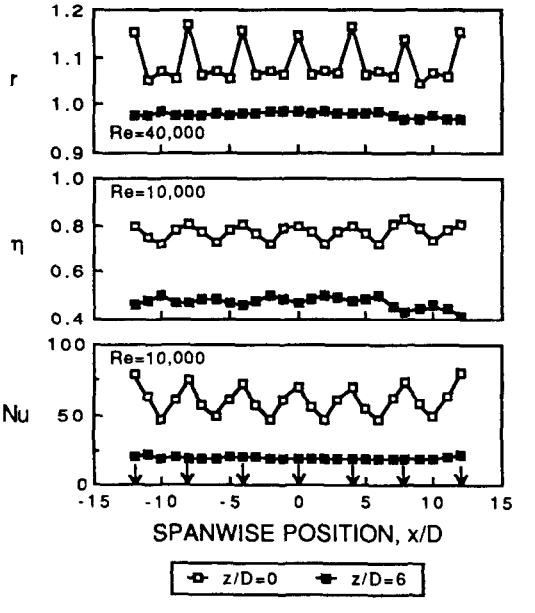

FIG. 2. Demonstration of spanwise symmetry, $L/D = 6$, $S/D = 4$.

test section. The graph shows the spanwise variations ($-12 \leqslant x/D \leqslant 12$) of the recovery factor, the effectiveness and the Nusselt number at $z/D = 0$ and 6. The arrows (↓) indicate the locations of the jet centerlines. The spanwise periodicity is excellent, and end effects are negligible for the inner 6–8 jets of the row of 16 jets. Although this is illustrated only for one geometric configuration ($L/D = 6$, $S/D = 4$), spanwise periodicity is good, and end effects are negligible for other configurations [27]. Therefore, the later experimental results are presented only for $-4 \leqslant x/D \leqslant 4$.

Recovery factor

All recovery factors are determined with a jet Reynolds number of about 40 000, which corresponds to the maximum mass flow rate the flow system can provide. A larger mass flow rate gives smaller experimental uncertainties. Several studies [2, 9, 29] show that the recovery factor is independent of the jet Reynolds number.

Figure 3 presents recovery factor distributions for the jet-to-plate distances (L/D) of 2, 4, 6 and 8 and the jet-to-jet spacings (S/D) of 4 and 8. The recovery factor varies from 0.8 to 1.2 in the range of the present study. There are large variations in the recovery factor distribution near the impingement region, while, far from the impingement line, the recovery factor approaches unity (as T_r approaches $T_\infty (= T_j^\circ)$). Although care is taken to set T_j° equal to T_∞, small variations in temperature with time produce the small offset of recovery factor from unity at the far downstream region ($z/D = 6$).

Considering the recovery factor distribution for $L/D = 2$ and $S/D = 8$, the recovery factor at the impingement point of each jet is approximately 0.95 with local minima on either side along the impingement line ($z/D = 0$). The occurrence of significant local minima in recovery factor at small L/D can be attributed to energy separation in the highly curved flow as discussed by Eckert [3]. Goldstein *et al.* [2] observed similar minima in recovery factor in a study with a single, circular, impinging jet, and explained that the phenomena was associated with energy separation due to the vortex rings surrounding the jet. At small jet-to-plate spacings where the impingement plate would be within the potential-core of the jet, the jet is surrounded by vortex rings. These vortex rings keep their orderly structure after impingement [30]. For vortex motion, as discussed by Hartnett and Eckert [31], an energy separation exists, where the minimum energy occurs at the center of the vortex. This corresponds to the local minima in recovery factor. For $L/D \geqslant 4$, breakdown of the vortex rings takes place [30], and the local minima of recovery factor tend to disappear.

For $L/D = 4$ and $S/D = 4$, along the impingement line ($z/D = 0$) the recovery factor has its maximum of approximately 1.07 at each impingement point, and a secondary maximum of approximately 1.05 occurs midway between the jets. Stagnation due to the 'collision' of the spreading flows from adjacent impinged jets is responsible for these secondary maxima. This interaction appears to be strong when the jets are closely spaced and the jet exit-to-plate distance is small.

The fact that the recovery factor in the impingement region is greater than unity for large jet-to-plate spacings ($L/D \geqslant 4$) may be explained as follows. Since the total temperature of the jet is set equal to the ambient temperature, the static temperature of the jet is lower than the ambient temperature by the jet dynamic temperature. As the air in jet travels through the ambient air, it is heated by entraining the warmer ambient air. This raises the stagnation temperature of the jet and hence the recovery factor. Supporting this view, the recovery factor at the impingement point increases with larger jet exit-to-plate distance which permits more entrainment of the ambient air into the jet. This behavior was also noted by Gardon and Cobonpue [1], Goldstein *et al.* [2] and Sparrow *et al.* [5].

Effectiveness

Most of the effectiveness data were taken with a jet Reynolds number of about 10 000 and a temperature difference ($T_j^\circ - T_\infty$) of about 6°C. Figures 4 and 5 show that the effectiveness is independent of ($T_j^\circ - T_\infty$) and jet Reynolds number, respectively. The small discrepancies from these figures may be due to experimental error. Goldstein *et al.* [29] showed that the effectiveness does not depend on either ($T_j^\circ - T_\infty$) or Re for a single, circular, impinging jet. Hollworth and Wilson [17] also showed that the radial distribution of dimensionless recovery temperature (adiabatic wall temperature according to the definitions of the present study) is essentially similar regardless of the jet exit velocity and the temperature mismatch ($T_j^\circ - T_\infty$).

Effectiveness distributions are shown in Fig. 6 for $L/D = 2$, 6 and $S/D = 4$, 8. The arrows (↓) in the figures indicate the locations of the jet centerlines. Measurements of spanwise (x/D) distributions of the effectiveness are made at five streamwise locations ($z/D = 0$, 1, 2, 4 and 6). The effectiveness depends on the jet-to-plate distance (L/D) and the jet-to-jet spacing (S/D). Generally, the effectiveness has a maximum at the impingement point and decreases as the jet travels along the plate away from the impingement point and entrains more room air.

The effect of L/D on effectiveness can be seen by comparing the effectiveness for small and large spacings. For the small spacing ($L/D = 2$), the impingement-point effectiveness is very close to one, implying that the core of the jet is almost unaffected by the entrainment of the room air. It should be noted that the jet orifice plate itself may lower the rate of fluid entrainment into the jet (the diameter of the jet exit is 6.35 mm and the width of the jet orifice plate is 25.4 mm). For the large spacing ($L/D = 6$), the impingement point effectiveness is approximately 0.8 for both

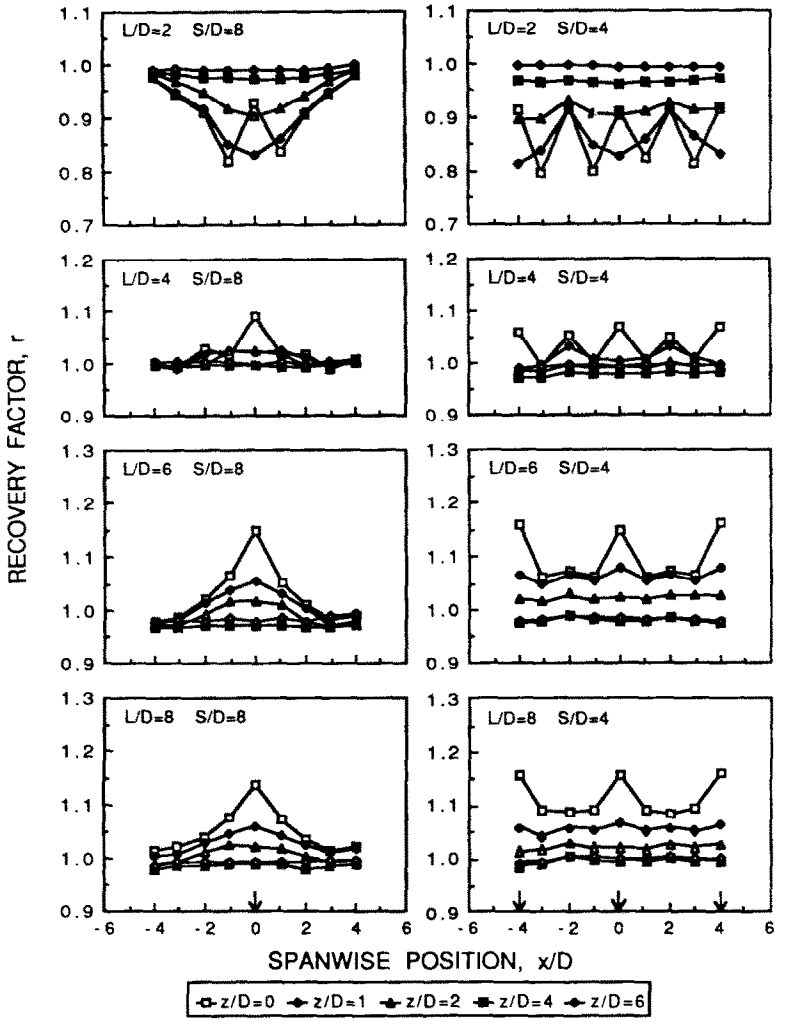

FIG. 3. Recovery factor distributions, $Re \approx 40\,000$.

$S/D = 8$ and 4. The jet entrains the ambient air as it travels from the jet exit to the impingement surface, and hence the adiabatic wall temperature is closer to the ambient.

The effectiveness is also influenced by the interaction between adjacent jets, which is expected to be stronger for the smaller jet-to-jet spacing. For the larger jet-to-jet spacing ($S/D = 8$), the local maxima in effectiveness occur at $x/D = 0$ for all streamwise locations ($z/D = 0$, 1, 2, 4 and 6). However, for the smaller jet-to-jet spacing ($S/D = 4$), local maxima occur at $x/D = 0$ and ± 4 (lines through the impingement points) for $z/D = 0$, 1 and 2, but they occur at $x/D = \pm 2$ (interaction lines of adjacent jets) for $z/D = 4$ and 6.

In Fig. 7, the effectiveness distributions for a slot jet, a single round jet, and a line of round jets are compared. The data for a heated slot jet are taken from Folayan and Whitelaw [14], and the data for a single jet are from Goldstein *et al.* [29]. The data from the present study for a single row of jets are for $x/D = 0$. As expected, the effectiveness for a single row of circular jets falls off more rapidly with z than that for a slot jet but more slowly than that for a single jet. Comparing the curves for a single row of jets, the decrease with increasing streamwise distance (z/D) is greater for the larger jet-to-jet spacing ($S/D = 8$) than for the smaller spacing ($S/D = 4$), which is evident when the jet-to-plate distance is small ($L/D = 2$). The single row of jets with the larger jet-to-jet spacing ($S/D = 8$) acts more like a single jet, and that with the smaller spacing ($S/D = 4$) acts more like a slot jet. When the jet-to-plate distance is relatively large ($L/D = 6$), the decay rates for the two jet-to-jet spacings are similar.

Local heat transfer coefficient

Figure 8 shows that the heat transfer coefficient defined in terms of the difference between the wall temperature and the adiabatic wall temperature is

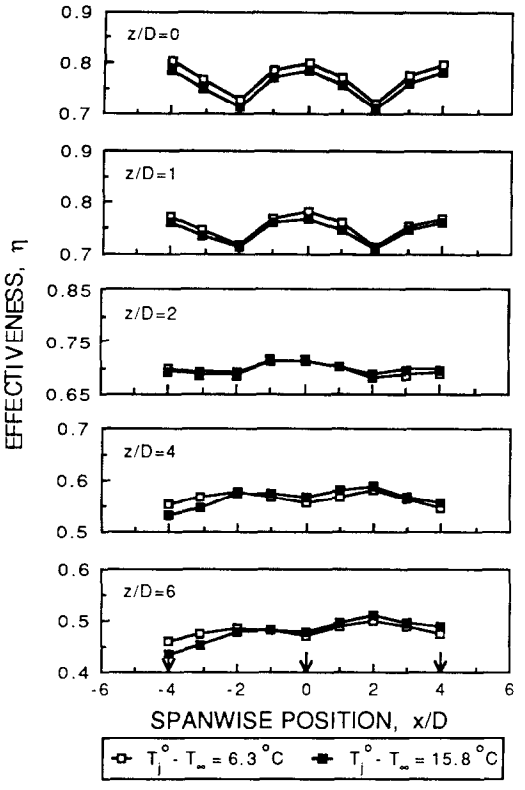

FIG. 4. Effectiveness distributions. Independence of $(T_j^\circ - T_\infty)$, $L/D = 6$, $S/D = 4$, $Re \approx 10\,000$.

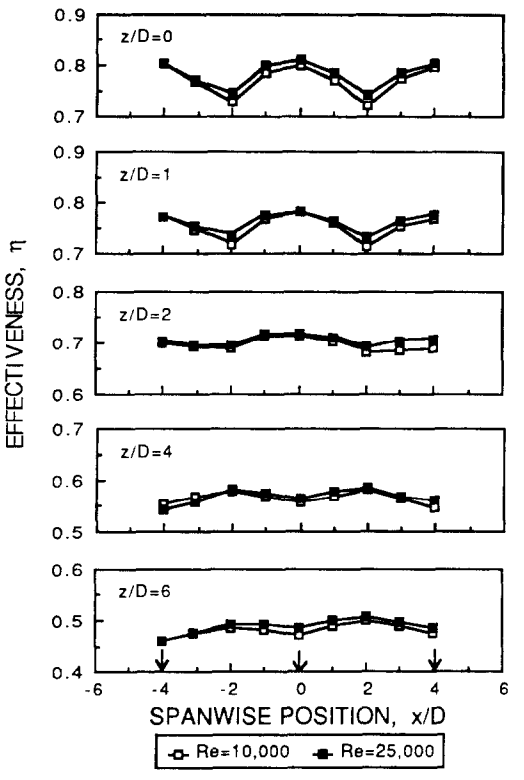

FIG. 5. Effectiveness distributions. Independence of Re, $L/D = 6$, $S/D = 4$.

independent of $(T_j^\circ - T_\infty)$ as noted by Goldstein *et al.* [29] and Hollworth and Gero [18] for a single, circular jet impinging upon a flat plate. Although this independence is shown only for $L/D = 6$, $S/D = 4$ and $Re = 20\,000$, it also holds for the other values of L/D, S/D and Re studied.

The distributions of local heat transfer coefficient contain a large amount of information, the extent of which is further enlarged by the presence of three independent parameters, Re, L/D and S/D. In general, the local Nusselt number would be a function of L/D, S/D, x/D, z/D, Pr (approximately constant in the present study), and Re. The dependence of Nusselt number on jet Reynolds number may be approximated by a power law dependence

$$Nu \propto Re^n.$$

The value of n is dependent on many factors, especially on the distance from the impingement point. Popiel *et al.* [13] proposed 0.5 for $2 < R/D < 5$ and 0.75 for $R/D > 5$ in their study with a single, circular jet, where R denotes the radial distance from the impingement point. Donaldson *et al.* [32] proposed 0.5 at the impingement point and 0.8 in the wall-jet region. Martin [26] proposed different values of n according to the range of jet Reynolds number. He proposed 0.57 for $2000 < Re < 30\,000$, 0.67 for $30\,000 < Re < 120\,000$ and 0.78 for $120\,000 < Re < 400\,000$.

A least square analysis was made to find a value of n which produces the best fit to the experimental data of the present study. According to the analysis [27], a smaller value (~ 0.67) fits the data at the impingement line ($z/D = 0$), whereas a larger value (~ 0.74) fits the data at downstream locations ($z/D = 4, 6$). For convenience, a single value of 0.7 is used in the present study. For a higher Reynolds number ($61\,000 < Re < 124\,000$) and a large range of radial distances ($0.5 \leqslant R/D \leqslant 32$), Goldstein *et al.* [2] used a constant value of 0.76 to correlate their experimental data.

Figure 9 shows spanwise distributions of $Nu/Re^{0.7}$ at various streamwise locations for the jet-to-plate distances (L/D) of 2 and 6, and the jet-to-jet spacings (S/D) of 4 and 8. Each figure contains results for nominal jet Reynolds numbers of 10 000, 20 000, 30 000, 40 000 when $S/D = 8$, or 10 000, 15 000, 20 000, 25 000 when $S/D = 4$. The arrows (↓) on the abscissa indicate the locations of the jet centerlines.

Examination of the figures reveals that local maxima occur at the impingement point of each jet, and local minima occur midway between the jets. It was found in several studies (e.g. refs. [23, 24]) that relative maxima (of the transfer coefficient) may exist

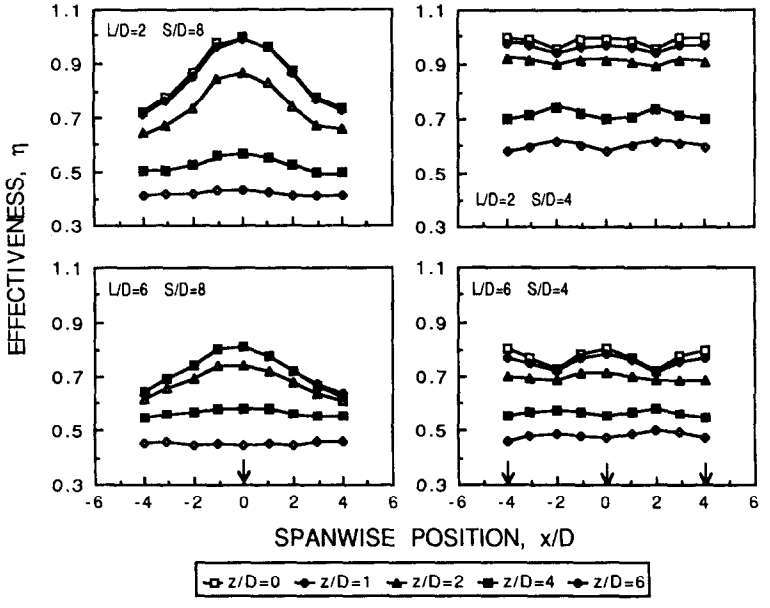

FIG. 6. Effectiveness distributions, $Re \approx 10\,000$.

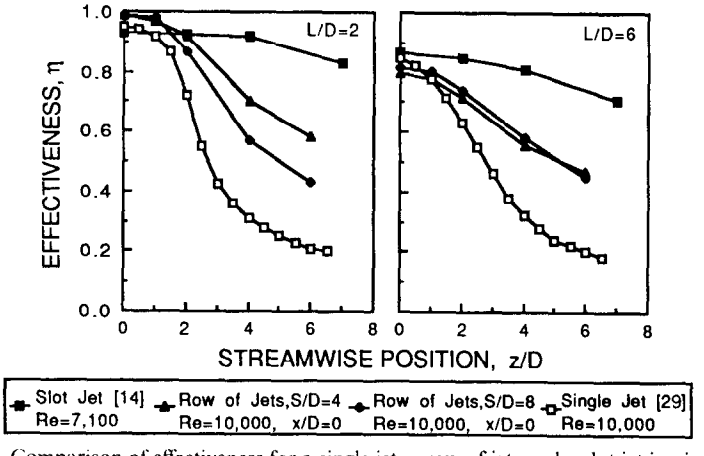

FIG. 7. Comparison of effectiveness for a single jet, a row of jets and a slot jet impingement.

midway between adjacent jets owing to the 'collision' of the spreading flows from adjacent impinged jets. In addition, local minima were observed at the stagnation points for a small jet-to-plate distance (e.g. $L/D = 2$) [1, 23, 24]. Neither the relative maxima between adjacent jets nor the local minima at the stagnation points were encountered in the present study. As noted by Goldstein and Timmers [24], with multiple jets, flow interaction can cause the mixing-induced turbulence to penetrate further towards the center of individual jets. This can cause the local minima at the stagnation points to be absent. The jet potential-core length in the present study would be very short due to the interference of the neighboring jets produced by square-edged orifices. It was also found by Popiel and Boguslawski [33] that the core of an orifice-produced jet is much shorter than that from a well-rounded nozzle jet. The absence of the relative maxima midway between adjacent jets may be due to the limited resolution of the present study (thermocouples are separated by one jet diameter).

The Nusselt number is largest on the impingement line ($z/D = 0$) and diminishes with increasing downstream distance, z. As z increases, the velocity tends to be more uniform (with x) due to the spreading of the impinged jets and the mixing of fluid from adjacent jets and the ambient. This results in a wall-jet flow which is eventually almost uniform across the span of the test plate; as a result, the spanwise distribution of the heat transfer coefficient becomes almost flat, and

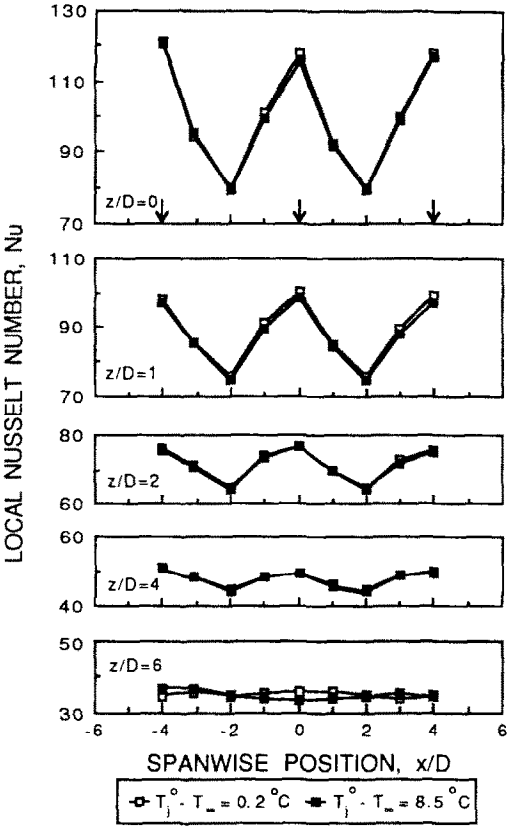

FIG. 8. Local Nusselt number distributions. Independence of $(T_j^\circ - T_\infty)$, $L/D = 6$, $S/D = 4$, $Re \approx 20000$.

the heat transfer diminishes in magnitude as the thickness of the wall-jet grows with increasing z/D. This is more evident when the jets are more closely spaced.

The local Nusselt number for $L/D = 2$ is slightly larger than that for $L/D = 6$. For example, when $S/D = 8$, $Nu/Re^{0.7}$ at the impingement point is about 0.11 for $L/D = 2$ and about 0.10 for $L/D = 6$. When $S/D = 4$, the difference in Nusselt number between $L/D = 2$ and 6 is much smaller, $Nu/Re^{0.7}$ being almost 0.12 for both.

The effect of L/D on the impingement point heat transfer has been studied by many researchers [1, 2, 5, 25, 34]. They observed that there is a maximum in the impingement point heat transfer coefficient at some L/D. The distance at which this maximum occurs depends on many parameters such as jet exit geometry, Re, etc.; however, it corresponds approximately to the length of jet potential-core. The value of L/D for maximum Nu in the present study cannot be determined from the available data, but it is probably quite short since, as noted before, the jet core length would be very short. Such a short jet exit-to-plate distance appears to be characteristic for maximum heat transfer from multiple jets, as contrasted to a single impinging jet, for which the maximum usually occurs at L/D of about 5–8 [1, 2].

Average heat transfer coefficient

Average Nusselt numbers are calculated from local Nusselt numbers using the trapezoidal rule for integration. Along lines of constant z/D, parallel to the impingement line, the spanwise-average Nusselt number is evaluated from the following equation:

$$\overline{Nu} = \frac{1}{x_2/D - x_1/D} \int_{x_1/D}^{x_2/D} Nu \, \mathrm{d}(x/D) \qquad (8)$$

where $x_1/D = 0$, $x_2/D = 4$. For both values of S/D (4 and 8) only the data points between $x_1/D = 0$ and $x_2/D = 4$ were used to evaluate the spanwise-average Nusselt number.

Figure 10 shows $\overline{Nu}/Re^{0.7}$ for $L/D = 2$ and 6 and $S/D = 4$ and 8. The spanwise-average Nusselt number has a maximum at the impingement line and decreases steadily with increasing distance (z) from the impingement line. The decay is faster for $S/D = 4$ than for $S/D = 8$. Since, for a given Re, the total mass flow rate for $S/D = 4$ is twice that for $S/D = 8$, the spanwise-average Nusselt number is larger for $S/D = 4$ than for $S/D = 8$. The difference in the spanwise-average Nusselt number between $S/D = 4$ and 8 is quite large at the impingement line and becomes smaller as z/D increases.

The solid line in the figure shows a correlation

$$\frac{\overline{Nu}}{Re^{0.7}} = \frac{2.9}{22.8 + (S/D)\sqrt{(L/D)}} \, \mathrm{e}^{-0.09(z/D)^{1.4}}. \qquad (9)$$

This correlation appears to be satisfactory in the range studied ($2 \leqslant L/D \leqslant 6$, $4 \leqslant S/D \leqslant 8$, $0 \leqslant z/D \leqslant 6$, $10000 \leqslant Re \leqslant 40000$).

Surface-average heat transfer coefficients are of importance, for example, when the plate to be heated or cooled is being moved beneath stationary jets. The speed at which the plate should be moved can be evaluated with the aid of the surface-average heat transfer coefficient. The surface-average Nusselt number from the impingement line ($z/D = 0$) to a particular streamwise (z/D) location is calculated from the following equation:

$$\overline{\overline{Nu}} = \frac{1}{z/D} \int_0^{z/D} Nu \, \mathrm{d}(z/D) \qquad (10)$$

Values of $\overline{\overline{Nu}}/Re^{0.7}$ for $L/D = 2$ and 6, and $S/D = 4$ and 8 are shown in Fig. 11. The streamwise coordinate, z/D, defines the downstream limit of the surface area over which the average is taken. The maximum of the surface-average Nusselt number occurs at the impingement line and, as the downstream limit for the averaging increases, the surface-average Nusselt number decreases monotonically. Like the spanwise-average Nusselt number, the surface-average Nusselt number for $S/D = 4$ decreases more rapidly than that for $S/D = 8$, and it is larger for the smaller jet-to-jet spacing.

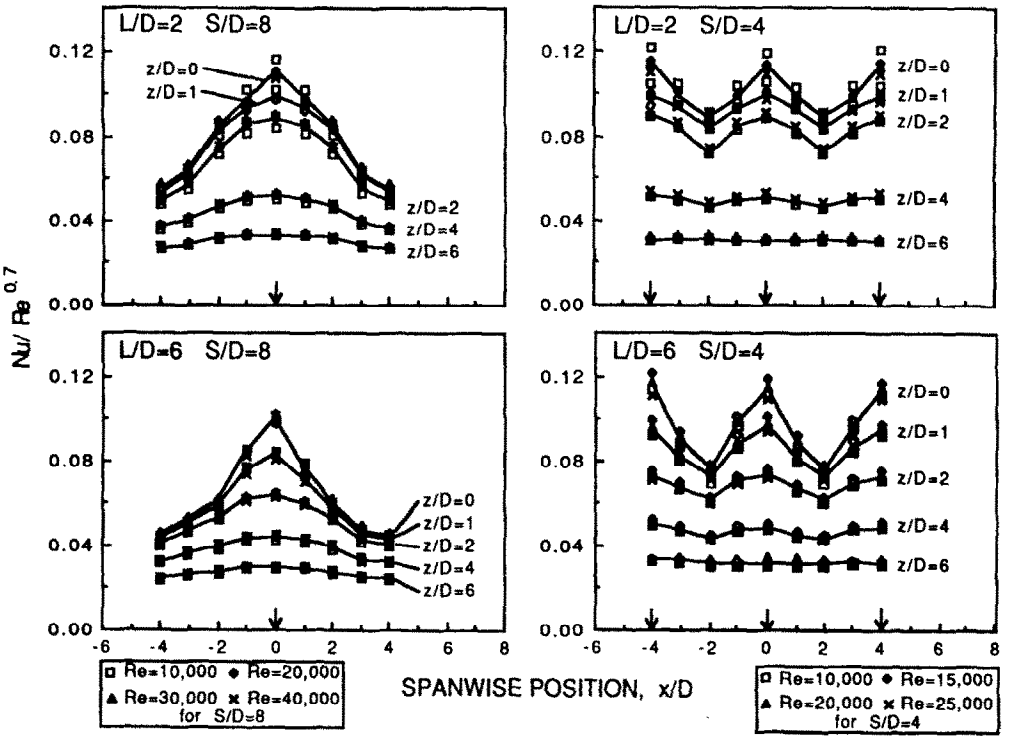

FIG. 9. Distributions of $Nu/Re^{0.7}$.

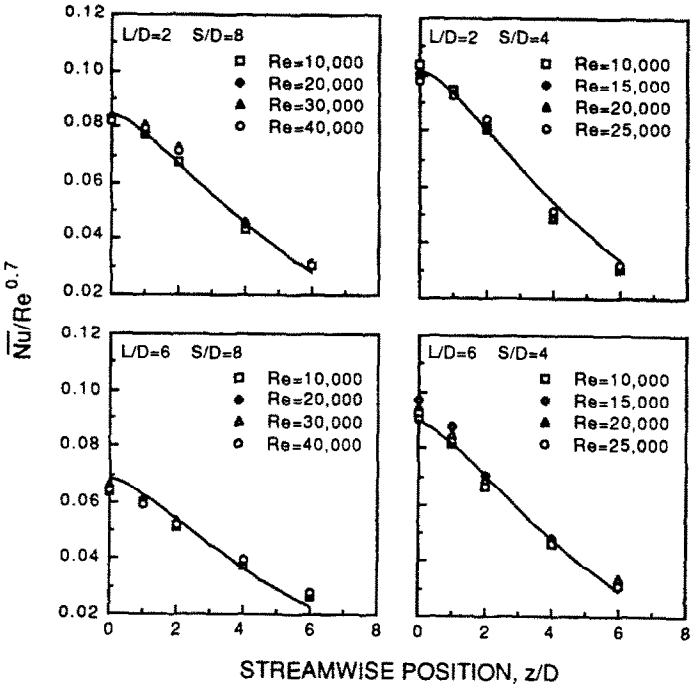

FIG. 10. Spanwise-average $Nu/Re^{0.7}$.

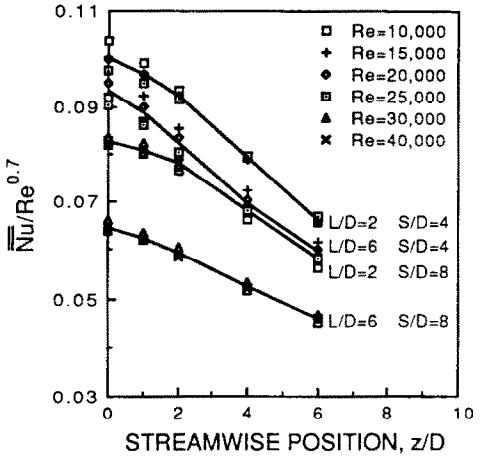

FIG. 11. Surface-average $Nu/Re^{0.7}$.

Comparison with other studies

Figure 12 shows a comparison of spanwise-average Nusselt numbers from the present study and spanwise-average Sherwood numbers from a mass transfer investigation by Koopman and Sparrow [23]. The mass transfer results may be converted to the heat transfer results by employing the heat–mass transfer analogy. According to the analogy, the conversion between the Sherwood and Nusselt number at the same Reynolds number can be accomplished using the correlation

$$Nu = Sh(Pr/Sc)^n \tag{11}$$

where n is usually 1/3 or 0.4. Taking $n = 0.4$, there is good agreement between the present study and that of ref. [23], especially in the wall-jet region.

In Fig. 13, the spanwise-average and the surface-average Nusselt numbers for a row of jets are compared to the similar average Sherwood numbers for an impinging slot jet taken from Martin [26]. Figure 13(a) shows a comparison at the same jet Reynolds number ($u_jD/\nu = u_jB/\nu$), and Fig. 13(b) shows a comparison at the same mass flow rate per unit span. When $S/D = 4$, a row of jets with $Re = 15000$ and a slot jet with $Re = 3000$ require almost the same mass flow rate per unit span. For the same jet Reynolds number, though the mass flow rate of a slot jet is larger than that of a row of jets (approximately five times when $S/D = 4$), a slot jet and a row of jets produce transfer coefficients of comparable magnitude. For the same mass flow rate per unit span, a row of jets produces much larger transfer coefficients than a slot jet. Thus a single row of circular jets appears to be more effective than a slot jet for maximizing the heat–mass transfer, especially in the impingement region.

CONCLUDING REMARKS

The effect of thermal entrainment on the impingement heat transfer for a single row of circular air jets may be characterized with the recovery factor, the effectiveness, and the Nusselt number.

The recovery factor is independent of jet Reynolds number, but is dependent on the jet exit-to-plate distance (L/D) and the jet-to-jet spacing (S/D). For small L/D and S/D ($L/D = 2$ or 4, and $S/D = 4$), the recovery factor has two peaks along the impingement line, one at the impingement point and the other at the secondary stagnation point due to the interaction between adjacent impinging jets. When the jet is very close to the impingement plate ($L/D = 2$), the recovery factor has local minima near $x/D \approx \pm 1$ along the impingement line, apparently due to energy separ-

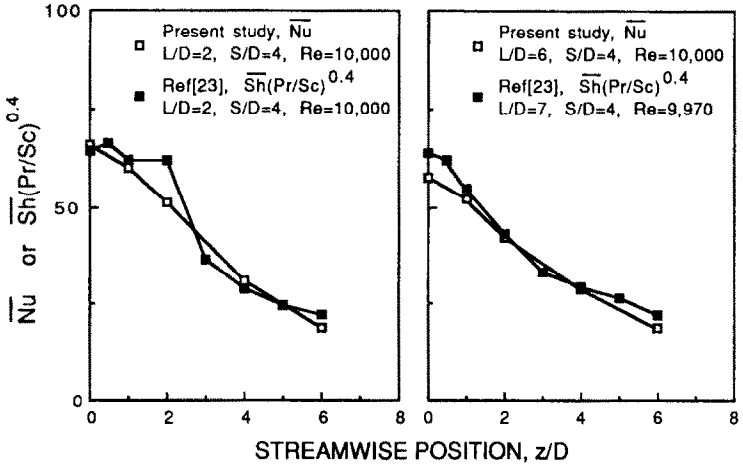

FIG. 12. Comparison of the spanwise average Nusselt number with other studies.

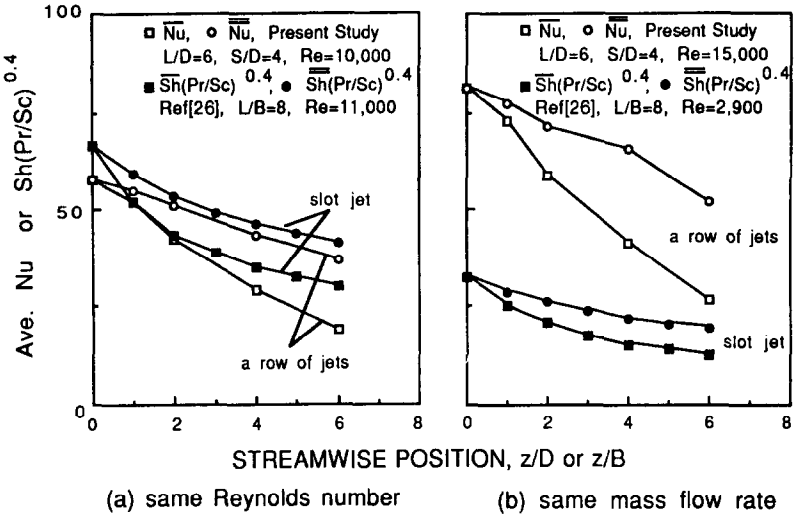

FIG. 13. Comparison of the spanwise and surface average Nusselt number with slot jet studies.

ation. When the jet exit-to-plate distance is large ($L/D \geqslant 4$), the impingement region recovery factor is larger than unity due to the entrainment of the ambient air into the jet flow. Far from the impingement point, the recovery factor approaches unity.

The effectiveness is independent of the jet Reynolds number and the temperature mismatch ($T_j^\circ - T_\infty$), but is dependent on the jet exit-to-plate distance (L/D) and the jet-to-jet spacing (S/D). It has a maximum at the impingement point and decreases as the jet entrains more ambient air with increasing downstream distance from the impingement point. The effectiveness for a larger jet-to-jet spacing (S) decreases more rapidly with increasing downstream distance. The impingement point effectiveness decreases with increasing jet exit-to-plate distance (L).

The heat transfer coefficient defined in terms of the difference between the wall temperature and the adiabatic wall temperature is independent of ($T_j^\circ - T_\infty$). The dependence of the Nusselt number on the jet Reynolds number can be approximated by a power law. The local heat transfer coefficient has a maximum at the impingement point and a minimum midway between adjacent jets. Both the spanwise-average Nusselt number and the surface-average Nusselt number have a maximum at the impingement line and decrease steadily with increasing downstream distance. At a given Reynolds number, the jets with the closer jet-to-jet spacing produce larger average Nusselt numbers. A single row of jets appears to be more efficient than a slot jet for maximizing the heat–mass transfer with the same mass flow rate.

Acknowledgement—Support for the conduct of this study from the Engineering Research Program of the Department of Energy is gratefully acknowledged.

REFERENCES

1. R. Gardon and J. Cobonpue, Heat transfer between a flat plate and jets of air impinging on it, *Proc. 2nd Int. Heat Transfer Conf.*, pp. 454–460. ASME, New York (1962).
2. R. J. Goldstein, A. I. Behbahani and K. Kieger Heppelmann, Streamwise distribution of the recovery factor and the local heat transfer coefficient to an impinging circular air jet, *Int. J. Heat Mass Transfer* **29,** 1227–1235 (1986).
3. E. R. G. Eckert, Cross transport of energy in fluid streams, *Thermo- and Fluid Dynam.* **21**(2–3), 73–81 (1987).
4. J. P. Bouchez and R. J. Goldstein, Impingement cooling from a circular jet in a cross flow, *Int. J. Heat Mass Transfer* **18,** 719–730 (1975).
5. E. M. Sparrow, R. J. Goldstein and M. A. Rouf, Effect of nozzle-surface separation distance on impingement heat transfer for a jet in a crossflow, *J. Heat Transfer* **97,** 528–533 (1975).
6. R. J. Goldstein and A. I. Behbahani, Impingement of a circular jet with and without cross flow, *Int. J. Heat Mass Transfer* **25,** 1377–1382 (1982).
7. B. R. Hollworth and R. D. Berry, Heat transfer from arrays of impinging jets with large jet to jet spacing, *J. Heat Transfer* **100,** 352–357 (1978).
8. A. I. Behbahani and R. J. Goldstein, Local heat transfer to staggered arrays of impinging circular air jets, *J. Engng Pwr* **105,** 354–360 (1983).
9. L. W. Florschuetz and C. C. Su, Recovery effects on heat transfer characteristics within an array of impinging jets. In *Heat Transfer and Fluid Flow in Rotating Machinery* (Edited by W. J. Yang), pp. 375–387. Hemisphere, Washington, DC (1987).
10. K. P. Perry, Heat transfer by convection from a hot gas jet to a plane surface, *Proc. Inst. Mech. Engrs*, London, Vol. 168, pp. 775–784 (1954).
11. G. C. Huang, Investigations of heat-transfer coefficients for air flow through round jets impinging normal to a heat-transfer surface, ASME Paper No. 62-HT-31 (1962).
12. J. Vlachopoulos and J. F. Tomich, Heat transfer from a turbulent hot air jet impinging normally on a flat plate, *Can. J. Chem. Engng* **49,** 462–466 (1971).

13. C. O. Popiel, T. H. van der Meer and C. J. Hoogendoorn, Convective heat transfer on a plate in an impinging round hot gas jet of low Reynolds number, *Int. J. Heat Mass Transfer* **23,** 1055–1068 (1980).
14. C. O. Folayan and J. H. Whitelaw, Impingement cooling and its application to combustor design, Tokyo Joint Gas Turbine Congress, Paper No. 7, JSME and ASME, Tokyo, Japan (1977).
15. S. A. Striegl and T. E. Diller, The effect of entrainment temperature on jet impingement heat transfer, *J. Heat Transfer* **106,** 27–33 (1984).
16. S. A. Striegl and T. E. Diller, An analysis of the effect of entrainment temperature on jet impingement heat transfer, *J. Heat Transfer* **106,** 804–810 (1984).
17. B. R. Hollworth and S. I. Wilson, Entrainment effects on impingement heat transfer: Part I—Measurements of heated jet velocity and temperature distributions and recovery temperatures on target surface, *J. Heat Transfer* **106,** 797–803 (1984).
18. B. R. Hollworth and L. R. Gero, Entrainment effects on impingement heat transfer: Part II—Local heat transfer measurements, *J. Heat Transfer* **107,** 910–915 (1985).
19. L. W. Florschuetz and C. C. Su, Effects of crossflow temperature on heat transfer within an array of impinging jets, *J. Heat Transfer* **109,** 74–82 (1987).
20. N. T. Obot, M. L. Graska and T. A. Trabold, The near field behavior of round jets at moderate Reynolds numbers, *Can. J. Chem. Engng* **62,** 587–593 (1984).
21. N. T. Obot, A. S. Majumdar and W. J. M. Douglas, The effect of nozzle geometry on impingement heat transfer under a round turbulent jet, ASME Paper No. 79-WA/HT-53 (1979).
22 D. E. Metzger, T. Yamashita and C. W. Jenkins, Impingement cooling of concave surfaces with lines of circular air jets, *J. Engng Pwr* **91,** 149–158 (1969).
23. R. N. Koopman and E. M. Sparrow, Local and average transfer coefficients due to an impinging row of jets, *Int. J. Heat Mass Transfer* **19,** 673–683 (1976).
24. R. J. Goldstein and J. F. Timmers, Visualization of heat transfer from arrays of impinging jets, *Int. J. Heat Mass Transfer* **25,** 1857–1868 (1982).
25. J. W. Gaunter, J. N. B. Livingood and P. Hrycak, Survey of literature on flow characteristics of a single turbulent jet impinging on a flat plate, NASA TN D-5652 (1970).
26. H. Martin, Heat and mass transfer between impinging gas jets and solid surfaces. In *Advances in Heat Transfer*, Vol. 13, pp. 1–60. Academic Press, New York (1977).
27. W. S. Seol, Heat transfer from a flat surface to a row of impinging circular air jets including the effect of entrainment, M.S. Thesis, University of Minnesota, Minneapolis, Minnesota (1987).
28. S. J. Kline and F. A. McClintock, Describing uncertainties in single sample experiment, *Mech. Engng* **75**(1), (1953).
29. R. J. Goldstein, K. A. Sobolik and W. S. Seol, Effect of entrainment on the heat transfer to a heated circular air jet impinging on a flat surface, *J. Heat Transfer* **112,** 608–611 (1990).
30. S. Yokobori, N. Kasagi, M. Hirata, M. Nakamaru and K. Haramura, Characteristic behavior of turbulence and transport phenomena at the stagnation region of an axisymmetrical impinging jet, 2nd Symp. on Turb. Shear Flows, Imperial College, London (July 1979).
31. J. P. Hartnett and E. R. G. Eckert, Experimental study of the velocity and temperature distribution in a high velocity vortex-type flow, *Trans. ASME* **79,** 751–758 (1957).
32. C. D. Donaldson, R. S. Snedeker and D. P. Margolis, A study of free jet impingement: Part 2. Free jet turbulent structure and impingement heat transfer, *J. Fluid Mech.* **45,** 477–512 (1971).
33. Cz. O. Popiel and L. Boguslawski, Mass or heat transfer in impinging single, round jets emitted by a bell-shaped nozzle and sharp-ended orifice, *Proc. 8th Int. Heat Transfer Conf.*, San Francisco, pp. 1187–1192 (1986).
34. R. Gardon and J. C. Akfirat, The role of turbulence in determining the heat-transfer characteristics of impinging jets, *Int. J. Heat Mass Transfer* **8,** 1261–1272 (1965).

TRANSFERT THERMIQUE POUR UNE RANGEE DE JETS CIRCULAIRES IMPACTANTS D'AIR, AVEC EFFET D'ENTRAINEMENT

Résumé—Une étude expérimentale est conduite pour caractériser le transfert thermique convectif à partir d'une surface plane pour une rangée de jets circulaires, impactants, submergés d'air formés par des orifices à bord carré ayant un rapport unité longueur/diamètre. On détermine les distributions du facteur de récupération, de l'efficacité et du coefficient de transfert thermique local. Les coefficients moyens de transfert sur la surface sont calculés à partir des coefficients locaux. Le coefficient de transfert est indépendant de la différence de température entre le jet et l'ambiance s'il est défini avec la différence entre la température de paroi (chauffée) et la température adiabatique à la paroi. L'efficacité est indépendante non seulement de cette différence de température mais aussi du nombre de Reynolds du jet dans le domaine étudié. Les coefficients moyens de transfert thermique ont les plus fortes valeurs sur la ligne d'impact et décroissent quand augmente la distance à celle-ci.

WÄRMEÜBERGANG AN EINE REIHE AUFTREFFENDER KREISRUNDER LUFTSTRAHLEN UNTER BERÜCKSICHTIGUNG DES ENTRAINMENT-EFFEKTES

Zusammenfassung—Der konvektive Wärmeübergang von einer ebenen Oberfläche an eine Reihe auftreffender kreisrunder Luftstrahlen, die durch scharfkantige Düsen mit einem Längen/Durchmesser-Verhältnis im Bereich von 1 erzeugt werden, wird untersucht. Die Verteilung folgender Größen wird bestimmt: Rückgewinnungsfaktor, Wirkungsgrad und örtlicher Wärmeübergangskoeffizient. Die örtlichen Wärmeübergangskoeffizienten werden über den Auftreffbereich der Strahlen sowie über die gesamte Oberfläche gemittelt. Der Wärmeübergangskoeffizient ist von der Temperaturdifferenz zwischen Strahl und Umgebung unabhängig, wenn er mit der Temperaturdifferenz zwischen den beheizten und den unbeheizten Teilen der Wand gebildet wird. Der Wirkungsgrad ist nicht nur von der Temperaturdifferenz zwischen Wand und Strahl unabhängig, sondern auch von der Reynolds-Zahl des Strahls im untersuchten Bereich. Die beiden Mittelwerte des Wärmeübergangskoeffizienten zeigen an der Auftrefflinie der Strahlen ein Maximum und nehmen mit zunehmender Entfernung von ihr ab.

ПЕРЕНОС ТЕПЛА К РЯДУ СТАЛКИВАЮЩИХСЯ ВОЗДУШНЫХ СТРУЙ КРУГЛОГО СЕЧЕНИЯ С УЧЕТОМ УВЛЕЧЕНИЯ

Аннотация—Экспериментально исследуется конвективный перенос тепла от плоской поверхности к ряду сталкивающихся затопленных воздушных струй круглого сечения, образованных каналами с отношением длины к диаметру, равным единице. Определяются распределения коэффициента восстановления, эффективности и локального коэффициента теплопереноса. На основе локальных коэффициентов теплопереноса рассчитываются коэффициенты, усредненные по струе и поверхности. Коэффициент теплопереноса, определяемый через разность между температурами нагреваемой и адиабатической стенок, не зависит от разности температур струи и окружающей среды. Эффективность не зависит не только от этой разности температур, но также от числа Рейнольдса струи в рассматриваемом интервале. Значения коэффициентов теплопереноса, усредненных по струе и поверхности, достигают максимума на линии соударения и уменьшаются с увеличением расстояния от нее.